Mon. Not. R. Astron. Soc. **390,** 323–330 (2008) doi:10.1111/j.1365-2966.2008.13735.x

Non-thermal processes in the cluster of galaxies Abell 3376

Anabella T. Araudo,[1,2,4]★ Sofía A. Cora[2,3,4] and Gustavo E. Romero[1,2,4]

[1]*Instituto Argentino de Radioastronomía (CCT La Plata, CONICET), C.C.5, 1894 Villa Elisa, Buenos Aires, Argentina*
[2]*Facultad de Ciencias Astronómicas y Geofísicas, Universidad Nacional de La Plata, Paseo del Bosque, B1900FWA La Plata, Argentina*
[3]*Instituto de Astrofísica de La Plata (CCT La Plata, CONICET, UNLP), Observatorio Astronómico, Paseo del Bosque, B1900FWA La Plata, Argentina*
[4]*Consejo Nacional de Investigaciones Científicas y Técnicas, Rivadavia 1917, Buenos Aires, Argentina*

Accepted 2008 July 20. Received 2008 July 8; in original form 2008 April 28

ABSTRACT

We model the high-energy emission that results from the interaction of relativistic particles with photons and matter in the cluster of galaxies Abell 3376. The presence of relativistic particles is inferred from the recently found radio relics in this cluster, being one of the most prominent examples of double opposite, giant ring-like radio structures. Assuming that diffusive shock acceleration takes place in the cluster regions where radio relics are observed, we calculate the spectral energy distribution resulting from the most relevant non-thermal processes, which are synchrotron radiation, inverse-Compton scattering, relativistic Bremsstrahlung and inelastic proton–proton collisions. In the context of our model, the major radiative component at high energies is inverse-Compton scattering, which could reach luminosities $L \sim 9 \times 10^{41}$ erg s^{-1} in the energy range between $\sim$1 MeV and 10 TeV. Hadronic interactions would yield a minor contribution to the overall non-thermal emission, but would dominate at ultrahigh energies. The cluster Abell 3376 might be detectable at gamma-rays by HESS, GLAST satellite and future planned Cherenkov arrays.

Key words: radiation mechanisms: non-thermal – galaxies: clusters: individual: Abell 3376 – gamma-rays: theory.

1 INTRODUCTION

Clusters of galaxies are characterized by thermal emission in the 2 to 10 keV soft X-ray region ($L_X \sim 10^{43}$–10^{45} erg s^{-1}) as a result of Bremsstrahlung radiation of the hot intracluster gas ($kT \sim 5$–8 keV). However, the detection of radiation at radio wavelengths (Feretti, Burigana & Enßlin 2004), as well as in the extreme ultraviolet (0.07–0.4 keV; EUV) (Bowyer et al. 2004) and at hard X-rays (20–80 keV; HXR) (Fusco-Femiano et al. 2004), indicates the presence of non-thermal activity in these systems. There is general consensus that radio emission is produced by synchrotron radiation originated from the interaction of relativistic electrons with the cluster magnetic field ($B \sim \mu$G) (Govoni & Feretti 2004). On the other hand, EUV radiation might be produced either by a cooler thermal component ($kT \sim 2$ keV) (Lieu et al. 1996; Mittaz et al. 1998) or by inverse-Compton (IC) scattering of cosmic microwave background (CMB) photons by the same population of relativistic electrons responsible for the radio emission (Enßlin & Biermann 1998; Lieu, Axford & Bonamente 1999). The latter process might also explain the HXR emission (Fusco-Femiano et al. 1999), although this possibility is still a matter of debate.

Regarding the radio emission, whose non-thermal origin is firmly established, clusters of galaxies present two different sources of diffuse large-scale synchrotron emission, known as 'radio haloes' and 'radio relics'. The former are located at the centre of clusters and characterized by unpolarized radio emission with structures that roughly resemble that shown by the X-ray emission, whereas the latter are polarized radio sources more irregularly shaped found at the periphery of clusters (e.g. Feretti & Giovannini 2008). Radio relics have been observed in several clusters. The most extended and powerful sources of this class have been detected in clusters with central radio haloes, such as Coma (Giovannini, Feretti & Stanghellini 1991) and Abell clusters A2163 (Feretti et al. 2001), A2255 (Feretti et al. 1997), A2256 (Röttgering et al. 1994) and A2744 (Govoni et al. 2001). Only few clusters present double opposite relics, being the most prominent examples those found in A3667 (Röttgering et al. 1997) and A3376 (Bagchi et al. 2006). The large radio flux recently detected from the relics of A3376 is an evidence of that relativistic leptons are present in those regions. For this reason, in this work we will be concerned with the non-thermal processes taking place in the outskirts of the cluster A3376 where the two giant and almost symmetric radio relics are located. Nevertheless, the model that we will present in this paper is also valid for clusters which present only one relic. In the case of A3376, the radio flux is more than one order the magnitude larger than in other radio emitting clusters, like A521 and A2163.

There is increasing evidence that the radio emitting particles in relics are accelerated by accretion and merger shocks generated in the intracluster medium (ICM) during cosmological large-scale structure formation. Because of the electron short radiative lifetimes, radio emission can be efficiently produced close to the

★E-mail: aaraudo@fcaglp.unlp.edu.ar

location of the shock waves. Thus, the origin of radio relics can be explained if they are considered to trace the position of these very large shocks (Enßlin et al. 1998; Hoeft, Brüeggen & Yepes 2004). According to the standard diffusive shock acceleration theory, shock waves in the presence of even modest and turbulent magnetic fields are sites of efficient acceleration of charged particles (Drury 1983). Another possibility may be adiabatic compression in these environmental shock waves (Enßlin & Gopal-Krishna 2001).

Based on the inferred population of high-energy particles involved in the previously mentioned non-thermal processes, it is natural to expect gamma-ray emission from galaxy clusters. This emission could be generated from neutral pion decay in cosmic ray collisions in the ICM (Völk, Aharonian & Breitschwerdt 1996), or by IC scattering that involves CMB photons and relativistic electrons (Atoyan & Völk 2000). Hydrodynamical cosmological simulations are a useful tool to estimate the properties of the cosmic ray populations in galaxy clusters and their effects on thermal cluster observables, as well as to predict the radiation emitted by these large virialized objects at gamma-ray energies (Keshet 2003; Pfrommer et al. 2007; Pfrommer, Enßlin & Springel 2008). A different numerical approach has been used by Berrington & Dermer (2003) to investigate the temporal evolution of particle and photon spectra resulting from non-thermal processes at the shock fronts formed in merging clusters of galaxies. All these works point to clusters, in general, as sources of gamma-ray emission observable with GLAST satellite.

These theoretical results are consistent with the fact that no gamma-ray emission has been detected so far with the current observational facilities, as indicated by the lack of correlations between unresolved EGRET gamma-ray sources and nearby X-ray bright galaxy clusters (Reimer et al. 2003). Only marginal evidence for emission from A1758 within the location error contours of the source 3EG J1337+5029 was reported by Fegan et al. (2005). Perseus and A2029 galaxy clusters were observed by Perkins (2006) with the Whipple 10-m Cherenkov telescope. They find no evidence of point source or extended gamma-ray emission in the TeV energy range. In addition, recent observations of the clusters Coma and A496 made by Domainko et al. (2007) with the array of Chrerenkov telescopes HESS have not detected significant signals of gamma-ray emission in exposure times of ∼10–20 h.

In this work, we estimate the high-energy emission of the recently detected radio relics in the nearby cluster A3376. Their radio power at 1.4 GHz, together with the assumption of an equipartition magnetic field, constrains effectively our model which is specific of this particular cluster. We assume a diffusive shock acceleration mechanism, and include different non-thermal processes that may be acting in the radio structures. We predict that the gamma-ray photons created in this cluster should be detected in the near future by GLAST, as well as by the new generation of Cherenkov arrays in the southern hemisphere, such as HESS II.

The paper is organized as follows. Section 2 describes the main features of the cluster A3376. Section 3 presents the acceleration and loss mechanisms that affect the content of relativistic particles in the ICM. The estimates of production of gamma-rays and lower energy radiation are given in Section 4. Finally, we summarize our results and present our concluding remarks in Section 5.

2 THE CLUSTER A3376

The rich cluster of galaxies A3376 has been detected by *ROSAT* and *XMM–Newton* through its X-ray emission revealing strong evidence for merger activity of subclusters. It has a X-ray luminosity $L_{\rm X}(0.1-2.4\,{\rm keV}) \simeq 1.22\times10^{44}\,h^{-2}\,{\rm erg\,s^{-1}}$. This power is produced by thermal Bremsstrahlung radiation from the hot ICM, which has an overall temperature $T_{\rm X}\approx 5.8\times10^{7}$ K (≈5 keV). This cluster is located in the southern hemisphere ($\alpha = 06^{\rm h}0^{\rm m}43^{\rm s}, \delta = -40^{\circ}03'$) at a redshift $z\approx0.046$, which corresponds to a distance of $d\sim197$ Mpc for a standard Λcold dark matter (ΛCDM) cosmology ($\Omega_{\rm m}=0.3, \Omega_{\Lambda}=0.7, H_0=100\,h\,{\rm km\,s^{-1}\,Mpc^{-1}}$, with $h=0.7$). The cluster mass has been estimated by applying the virial theorem to the cluster member galaxies, assuming that mass follows the galaxy distribution (Girardi et. al 1998), giving a virial mass $M_{\rm vir}\sim 3.64\times10^{14}\,h^{-1}\,{\rm M_{\odot}}$. The corresponding virial radius is $R_{\rm vir}\sim 0.98\,h^{-1}$ Mpc.

Radio observations made by Bagchi et al. (2006) with the Very Large Array (VLA) instrument show the presence of two giant, ring-shaped structures in the periphery of the cluster at a distance of $\sim0.7\,h^{-1}$ Mpc from its centre. The radio flux detected at $\nu=1.4$ GHz is $F_{\nu}=302$ mJy, which corresponds to a radio luminosity of $1.03\times10^{40}\,h^{-2}\,{\rm erg\,s^{-1}}$. These structures have features typical of radio relics (Giovannini & Ferreti 2004). They fit quite well on a projected ellipse with minor and major axes of ∼1.1 and $\sim1.4\,h^{-1}$ Mpc, respectively. Adopting a line-of-sight depth of $\sim189\,h^{-1}$ kpc, as Bagchi et al. (2006), the three-dimensional ellipsoid has a volume $V\sim0.15\,h^{-3}\,{\rm Mpc^3}$. From the composite map of radio and X-ray emissions shown by Bagchi et al. (2006) (see their fig. 1a), we infer that only ∼20 per cent of this volume is filled by the radio relics (i.e. $V_{\rm relic}\sim0.003\,h^{-3}\,{\rm Mpc^3}$).

Some physical parameters of the cluster, relevant for the purpose of this work, are not provided by the observations but can be obtained from simulations; in concrete, the gas density in the relics, $n_{\rm H}$, and the shock velocity, $v_{\rm s}$. We consider a cosmological non-radiative hydrodynamical *N*-body/smoothed particle hydrodynamics (SPH) resimulation of a galaxy cluster that has been initially selected from a dark matter simulation for a standard ΛCDM cosmology with $\Omega_0=0.3, h=0.7, \sigma_8=0.9$ and $\Omega_{\rm b}=0.04$ (Dolag et al. 2005). The presence of radio relics in A3376 might be interpreted as the result of an on-going merger of subclusters (Enßlin et al. 1998). Thus, the chosen simulated cluster has similar dynamical state as the observed one; it has a virial mass $M_{\rm vir}\sim1.4\times10^{14}\,h^{-1}\,{\rm M_{\odot}}$. From the analysis of this simulation, we obtain $n_{\rm H}\simeq2\times10^{-5}\,{\rm cm^{-3}}$ and $v_{\rm s}\simeq 1000\,{\rm km\,s^{-1}}$. Considering that the temperature of the ICM, where the shock is propagating, is $T_{\rm ICM}\sim10^{-1}\,T_{\rm relic}$ (Hoeft et al. 2004) the Mach number results $M\sim4.2$ (Gabici & Blasi 2003). For the rest of the paper, we express all numerical values adopting $h=0.7$.

3 CONTENT OF RELATIVISTIC PARTICLES

Shock waves generated during the formation and evolution of galaxy clusters are the main source for thermalization of the intracluster gas and the acceleration of particles (Pfrommer et al. 2006). The activity of radio galaxies embedded in the clusters also contributes to the population of relativistic particles, leaving fossil radio plasma that is detected as cavities in X-ray surface brightness maps (e.g. Churazov et al. 2000). Two radio galaxies have been observed in the cluster A3376. The radio source MRC 0600-399 is associated with the second brightest cluster member galaxy, and the other radio source is possibly originated from an elliptical galaxy. These radio galaxies are located within the central region of the cluster from where thermal Bremsstrahlung emission is detected. Therefore, we can consider that the ring-shape radio structures present in the periphery of the cluster are not connected with these point sources.

The morphology of the X-ray and radio emission observed in the cluster A3376 suggests that it is undergoing a merger. As numerical simulations show (e.g. Hoeft et al. 2004), shock waves propagate in both directions along the line that connects the centres of the merging clusters, with the radio relics observed almost exclusively at the location of the shock fronts. Thus, particle acceleration induced by shock waves generated during this process is a suitable scenario for explaining the origin of the relics.

Taking into account the observational evidences and numerical results, we assume that the content of relativistic particles in the relics arises as a result of the acceleration by mergers shocks, neglecting the possible contribution of the radio galaxies. In the following sections, we describe the acceleration processes and losses that affect both electrons and protons, which determine the particle distributions and their subsequent evolution.

3.1 Acceleration and losses

The diffuse radio emission produced at the location of relics supports the presence of relativistic electrons and magnetic fields. Although there is no observational evidence of the existence of relativistic protons in the radio relics, these particles could be accelerated in the same way as electrons are.

We focus here on the acceleration of particles at the (non-relativistic) shock front via a diffusive process, such as first-order Fermi mechanism. In this theory, the time-scale related to the rate of energy gain of particles is

$$\tau_{\rm gain} = \frac{\gamma}{\dot{\gamma}_{\rm gain}} = \frac{\eta\, E}{e\, B\, c}, \tag{1}$$

where γ is the Lorentz factor and E is the energy ($E = \gamma mc^2$) up to which the particle, electron or proton, is accelerated; B is the magnetic field. The parameter $\eta = 2\pi f_{\rm sc}(c/v_{\rm s})^2$ involves the velocity of the shock, $v_{\rm s}$, and the ratio $f_{\rm sc}$ between the mean free path of the particle and its gyroradius; the latter can be expressed as $r_{\rm g} = E({\rm eV})/[300\, Z\, B({\rm G})]$, being Z the charge number of the particle. For the shock velocity, we assume a typical value of $v_{\rm s} \sim 1000\,{\rm km\,s^{-1}}$, as it is inferred from the analysis of our cluster simulation, being in agreement with general simulations results (e.g. Pfrommer et al. 2006). Then assuming Bohm diffusion (i.e. $f_{\rm sc} = 1$), we have $\eta = 5.7 \times 10^5$.

The rate of accelerated particles, $Q(\gamma)$, injected in the source follows a power-law energy distribution with a spectral index $\Gamma = 2.1$, typical of a diffusive acceleration mechanism and in accordance with the estimated Mach number M (see Blasi 2003 for similar values of the spectral index in Coma cluster). Once the accelerated particles are injected, their spectral energy distributions evolve as a consequence of radiative and advection losses. The latter refers to the escape of particles from the acceleration region.

In order to study the time evolution of the energy distribution of particles, we need to calculate the leptonic and hadronic radiative losses. In the following, we refer as primary particles to those relativistic particles that have been accelerated at the shock front by the Fermi-like mechanism. Secondary particles are the products originated from the interactions suffered by relativistic protons with target thermal protons of the ICM. These inelastic proton–proton (pp) collisions are the main channel of hadronic losses.

The cooling rate of relativistic protons as a result of pp interactions can be estimated by

$$\dot{\gamma}_{pp} = -4.5 \times 10^{-16} n_{\rm H} \left[0.95 + 0.06 \ln\left(\frac{\gamma}{1.1}\right)\right] \gamma \ \ {\rm s^{-1}} \tag{2}$$

(Mannheim & Schlickeiser 1994), where γ is the Lorentz factor for protons and $n_{\rm H}$ is the average hydrogen density of the relics obtained from the simulation. Part of the energy lost by relativistic protons is used to create neutral pions which subsequently decay into gamma-rays. The rest is used in the creation of charged pions that will decay finally producing electron–positron pairs ($e^{\pm}$) and neutrinos. The secondary pairs are cooled by the same radiative processes that affect primary electrons. Lepton energy losses are estimated taking into account relativistic Bremsstrahlung, IC interactions and synchrotron radiation (e.g. Ginzburg & Syrovatskii 1964).

Since the ICM is fully ionized, we consider Bremsstrahlung losses for bared nuclei, which are given by

$$\dot{\gamma}_{\rm Br} = -6.9 \times 10^{-17} n_{\rm H} Z^2 (\ln\gamma + 0.36)\gamma \ \ {\rm s^{-1}}. \tag{3}$$

Losses due to IC interactions depend on the energy density of photons, $U_{\rm ph}$. In the Thomson regime, they are given by

$$\dot{\gamma}_{\rm IC} = -3.2 \times 10^{-8}\, U_{\rm ph}\, \gamma^2 \ \ {\rm s^{-1}}. \tag{4}$$

The two photon fields relevant for the physical processes taking place in clusters of galaxies are the CMB radiation and thermal X-ray photons originated within the ICM itself through thermal Bremsstrahlung. The former is given by $U_{\rm CMB} = a\, T^4\, c^{-1}\, (1+z)^4$, where a is the Stefan–Boltzmann constant and $T = 2.725$ K is the CMB temperature; thus, $U_{\rm CMB} = 1.2 \times 10^{-13}\,{\rm erg\,cm^{-3}}$ at the cluster redshift. The latter is expressed as $U_{\rm X} = L_{\rm X}(4\pi R^2\, c)^{-1}\, (1+z)^4$, where $L_{\rm X}$ is the X-ray luminosity and R is the radius from which this luminosity is measured, which is about ∼0.15–0.3 per cent of the virial radius (Balestra et al. 2007). In the case of the cluster under study, $L_{\rm X} \simeq 2.44 \times 10^{48}\,{\rm erg\,s^{-1}}$ and $R \approx 0.3$ Mpc, giving $U_{\rm X} \approx 1.3 \times 10^{-15}\,{\rm erg\,cm^{-3}}$. Since $U_{\rm X}$ is two orders of magnitude lower than $U_{\rm CMB}$, we can consider $U_{\rm X}$ negligible (in both Thomson and Klein–Nishina regimes of IC interactions) and $U_{\rm ph} \sim U_{\rm CMB}$. Taking into account the energy for which the emission of the CMB spectrum reaches its maximum ($E_{\rm CMB} \sim 1.9 \times 10^{-4}$ eV), leptons should reach energies greater than 1.6×10^{15} eV in order to satisfy the condition $\xi = E_{\rm e} E_{\rm CMB}/(m_{\rm e}c^2)^2 \geq 1$, that defines the Klein–Nishina regime of the IC interactions. As we show in Section 3.2, these high energies are never achieved by primary electrons; hence, IC scattering develops in Thomson regime.

Losses produced by synchrotron radiation are computed as

$$\dot{\gamma}_{\rm synch} = -1.9 \times 10^{-9} B^2\, \gamma^2 \ \ {\rm s^{-1}}. \tag{5}$$

The calculation of synchrotron losses requires the knowledge of magnetic field, B. We estimate B by assuming equipartition between the energy density of the magnetic field and the relativistic particles, that is,

$$\frac{B^2}{8\pi} = u_{\rm e_1} + u_{\rm p} + u_{\rm e_2}, \tag{6}$$

where $u_{\rm e_1}$ and $u_{\rm e_2}$ are the energy densities of primary electrons and secondary pairs, respectively, and $u_{\rm p}$ is the energy density of protons. The energy density of i-particles ($i = e_1, p, e_2$) is expressed as

$$u_i = \int_{E_i^{\rm min}}^{E_i^{\rm max}} E_i\, n(E_i)\, {\rm d}E_i, \tag{7}$$

where $n(E_i)$ is the particle energy distribution. For protons, $n(E_{\rm p}) = K_{\rm p} E_{\rm p}^{-2.1} \exp(-E_{\rm p}/E_{\rm p}^{\rm max})$ but for leptons $n(E_{\rm e_{1,2}})$ is a broken power law:

$$n(E_{\rm e}) = \begin{cases} K_{\rm e}\, E_{\rm e}^{-\Gamma_{\rm e}} & E_{\rm e} \leq E_{\rm b} \\ K'_{\rm e}\, E_{\rm e}^{-\Gamma_{\rm e}-1}\, \exp(-E_{\rm e}/E_{\rm e}^{\rm max}) & E_{\rm e} \geq E_{\rm b}. \end{cases} \tag{8}$$

Table 1. Magnetic field, B, and normalization constant of the energy distribution of primary accelerated electrons, K_{e_1}, and protons, K_p, for the three different cases considered characterized by the parameter a.

a	B (G)	K_{e_1} (erg$^{\Gamma-1}$ cm^{-3})	K_p (erg$^{\Gamma-1}$ cm^{-3})
0	9×10^{-7}	1.4×10^{-15}	–
1	1.1×10^{-6}	1.1×10^{-15}	8.7×10^{-16}
100	3.4×10^{-6}	3×10^{-16}	2.5×10^{-14}

Table 2. Maximum energies obtained for primary electrons and protons accelerated in the radio relics of A3376 are given in the first and second columns, respectively. The maximum energy for secondary pairs $e^{\pm}$ is presented in the last column.

a	$E_{e_1}^{max}$ (eV)	E_p^{max} (eV)	$E_{e_2}^{max}$ (eV)
0	9×10^{13}	–	–
1	9.3×10^{13}	5.0×10^{17}	4×10^{16}
100	8.8×10^{13}	1.3×10^{18}	10^{17}

The spectral indices are $\Gamma_{e_1} = 2.1$ for primary electrons and $\Gamma_{e_2} = 2.08$ for secondary pairs; E_b is the break energy (see Section 3.3 for the estimation of E_b and K'_e). In all the cases, E_i^{max} is the maximum energy that particles can reach that depends on the mechanism of energy gain and losses that affect the particles. The contribution of E_i^{max} to integral equation (7) can be neglected because the slope of the particle distributions is negative: $n(E_i) \propto E_i^{-\Gamma_i}$. On the other hand, we assume a minimum energy $E_{e_1}^{min} = 1$ MeV for primary electrons and $E_p^{min} = 1$ GeV for protons. Thus, for secondary pairs we estimated $E_{e_2}^{min} \sim E_p^{min}/6 \sim 0.17$ GeV. Since the number of accelerated protons is unknown, we consider $u_p = a u_{e_1}$, where a is a free parameter in our model. We adopt three different values: $a = 0$ (no proton acceleration), $a = 1$ (equal energy density in protons and in electrons) and $a = 100$ (protons dominate the energy density budget).

Efficient production of secondary electrons requires a dense population of thermal protons as a target. However, this condition is not found at the peripheral cluster regions which are characterized by low-density gas ($n_H \sim 10^{-5}$ cm^{-3}). Therefore, the contribution of secondary pairs to the total energy density (equation 6) is neglected. Then, applying the constraint of the radio flux observed for A3376 ($F_\nu = 302$ mJy), we estimate the magnetic field and the normalization constant of the energy distribution of primary accelerated electrons, K_{e_1}, and protons, K_p. The results are shown in Table 1. Using the estimated spectral energy distribution of protons, we obtain a ratio between energy densities $u_{e_2}/u_p \sim 10^{-5}$, which justifies our previous assumption about the secondaries.

3.2 Maximum energies

The theoretical maximum energy of primary particles is determined by the competition between the rates of energy gain and losses, as described in the previous section. Fig. 1 shows the time-scales of energy losses of primary electrons as a function of their energy (equations 3–5). These time-scales are compared with the one corresponding to the acceleration rate, given by equation (1). From this comparison, we obtain the maximum energy allowed for electrons,

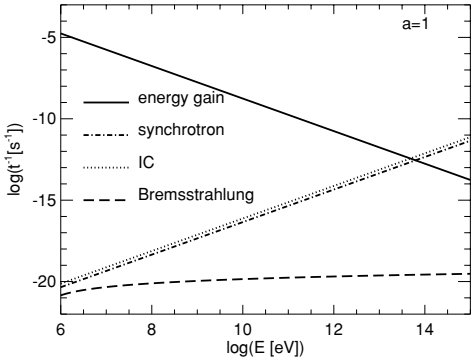

Figure 1. Rate of energy gain of primary electrons for $\eta \sim 5.7 \times 10^5$ compared with energy-loss rates obtained for the case $a = 1$.

$E_{e_1}^{max}$, which is $\sim 9 \times 10^{13}$ eV. For the case of protons, we take into account the energy-loss rate given by *pp* interactions (equation 2), considering that they have the same acceleration rate as electrons. We estimate proton maximum energies $E_p^{max} \simeq 1.8 \times 10^{21}$ and 4.6×10^{21} eV for cases with $a = 1$ and 100, respectively. At proton energies higher than $\sim 5 \times 10^{18}$ eV, photopair production against CMB photons starts to be important, and beyond energies of $\sim 5 \times 10^{19}$ eV photopion losses become dominant (e.g. Berezinsky & Grigoreva 1988; Kelner & Aharonian 2008). However, in the current analysis we do not need to take these losses into account since, as we will see below, the actual maximum energy of protons in the relics will be determined by additional constraints.

The values of maximum energy found for both electrons and protons are valid as long as they allow the particles to remain within the acceleration region. Thus, the particles have to satisfy the constraint $r_g < l$, where r_g is the gyroradius of the particle and l is the size of the acceleration region. By assuming that the particles are accelerated by the shock waves traced by the observed radio relics, we adopt the approximation $l \simeq l_{relic} \sim 0.3$ Mpc; this value is obtained from the examination of the projected radio map of the cluster A3376. For the electrons with energies close to the maximum value $E_{e_1}^{max}$, we find that $r_g \sim 0.1$ pc. Thus, the most energetic electrons are contained within the acceleration region. The situation for protons is different since the corresponding maximum energy, E_p^{max}, makes their gyroradius larger than l_{relic}. Hence, E_p^{max} is determined from the condition $r_g = l_{relic}$. This estimation gives $E_p^{max} \simeq 9.7 \times 10^{19}$ and 2.6×10^{20} eV, for $a = 1$ and 100, respectively. However, the time required for protons to reach these energies is higher than the lifetime of the relic ($\tau_{shock}^{relic} \sim 1$ Gyr; see the next section). Thus, the actual maximum energy to which protons can be accelerated is obtained equating τ_{acc} and τ_{relic}. The resulting values of E_p^{max} obtained from this constraint are lower, being $\sim 5 \times 10^{17}$ and $\sim 1.3 \times 10^{18}$ eV for $a = 1$ and 100, respectively.

The contribution of secondary pairs to the total spectral energy distribution (SED) will be taken into account even though the ambient conditions at the cluster outskirts are not favourable for the generation of these particles through *pp* interactions. To this aim, we first calculate the injected spectrum of secondary pairs taking into account the estimated distribution of relativistic protons, $n(E_p)$, and the new parametrization of the inelastic cross-section of *pp* interactions

$$\sigma_{inel}(E_p) = 34.3 + 1.88L + 0.25L^2 \text{ mb} \quad (9)$$

given by Kelner, Aharonian & Vugayov (2006), where $L = \ln(E_p/1\,\text{TeV})$. The maximum energies for secondary pairs are

assumed to be equal to the maximum energy of the photons produced by π^0-decay (Kelner et al. 2006, fig. 12). In Table 2, the maximum energies achieved by primary electrons, protons and secondary pairs are shown.

We now analyse the time evolution of the spectral energy distribution of the three kind of relativistic particles present in the radio relics.

3.3 Time evolution of the energy distributions of relativistic particles

Relativistic particles are injected in the radio emitting region of the cluster with an energy distribution that follows a power law, which subsequently evolves as a consequence of the radiative losses suffered by the particles. Such evolution is estimated, as a first-order approximation, by adopting a model in which the energy distribution of the particles is determined by the following transport equation

$$\partial n(t,\gamma)/\partial t + \partial \dot{\gamma} n(t,\gamma)/\partial\gamma + n(t,\gamma)/\tau_{\rm esc} = Q(t,\gamma) \qquad (10)$$

(e.g. Khangulyan et al. 2007), where t is the time, $Q(t,\gamma)$ is the particle injection function, which for present case will be time independent and $\tau_{\rm esc}$ is the advection escape time defined as $\tau_{\rm esc} = l_{\rm relic}/v_{\rm adv}$. In the shock rest frame, the downstream (post-shock) plasma velocity is given by $v_{\rm adv} \sim v_{\rm shock}/4$; thus, we obtain $\tau_{\rm esc} \sim$ 1.1 Gyr.

Particles are injected into the relics with a rate $Q(\gamma)$ as the shock wave propagates from the centre of the cluster up to the location of the relics. For the purpose of this work, the variable t corresponds to different values of the lifetime of the shock, $\tau_{\rm shock}$. When the shock reaches the location of the observed radio relics, this lifetime is referred to as $\tau^{\rm relic}_{\rm shock}$. From the assumed shock velocity $v_{\rm s} \sim 1000\,{\rm km\,s^{-1}}$ (Section 3.1) and the position of the observed radio relics in cluster A3376, we have $\tau^{\rm relic}_{\rm shock} \sim 0.95$ Gyr. This value is consistent with the one obtained from numerical simulations of cluster mergers (e.g. Hoeft et al. 2004).

The time-derivative $\dot{\gamma}$ is a function accounting for all the energy losses affecting leptons and protons, that is, mainly synchrotron and IC interactions in the former case and *pp* interactions in the latter one. The solution of equation (10) for different shock lifetimes is

$$n(\gamma) = \frac{1}{|\dot{\gamma}|}\int_{\gamma}^{\gamma_{\rm eff}} Q(\gamma')\mathrm{e}^{-\tau(\gamma,\gamma')/\tau_{\rm esc}}\mathrm{d}\gamma', \qquad (11)$$

where $\gamma_{\rm eff}$ and $\tau(\gamma,\gamma')$ are determined by

$$\tau_{\rm shock} = \int_{\gamma}^{\gamma_{\rm eff}} \frac{\mathrm{d}\gamma'}{|\dot{\gamma}'|} \quad \text{and} \quad \tau(\gamma,\gamma') = \int_{\gamma}^{\gamma'} \frac{\mathrm{d}\gamma''}{|\dot{\gamma}''|}. \qquad (12)$$

The cooling time of leptons is $\tau_{\rm cool} = \gamma/\dot{\gamma}_{\rm loss} \sim 2\times10^{20}\gamma^{-1}$ s. If $\tau_{\rm cool} > \tau_{\rm shock}$ at a certain energy, the particle energy distribution has the shape characterized by $\Gamma_{\rm e} = \Gamma$ and $K_{\rm e}$ (see Table 1). There is a break energy, $E_{\rm b}$, above of which $\tau_{\rm cool} < \tau_{\rm shock}$. In this case, both primary electrons and secondary pairs suffer radiative losses that affect the injected particle spectrum. As a consequence of this, the cooled spectrum has an index $\Gamma'_{\rm e_{1,2}} = \Gamma_{\rm e_{1,2}} + 1$ with a normalization constant $K'_{\rm e_{1,2}} \sim E_{\rm b}K_{\rm e_{1,2}}$ for energies $E_{\rm e_{1,2}} > E_{\rm b}$. The computed particle energy distributions of primary electrons and secondary pairs are shown in Fig. 2. As can be seen, the spectrum is broken at $E_{\rm b} \sim 5\times10^9$–$5\times10^{10}$ eV for values of $\tau_{\rm shock}$ comprised in the range 100 Myr to 1 Gyr, being the break energies smaller for larger lifetimes of the shock.

In this scenario, particles will reach the steady regime when $\tau_{\rm shock} \geq \tau_{\rm esc}$. For this reason, as $\tau^{\rm relic}_{\rm shock} \sim \tau_{\rm esc}$, we can consider that by the time when the radio relic is observed, the particle energy distribution $n(\gamma)$ is already steady.

Regarding protons, the escape time-scale ($\tau_{\rm esc} \sim 1.1$ Gyr) and shock lifetime ($\tau^{\rm relic}_{\rm shock} \sim 1$ Gyr) are shorter than the cooling time

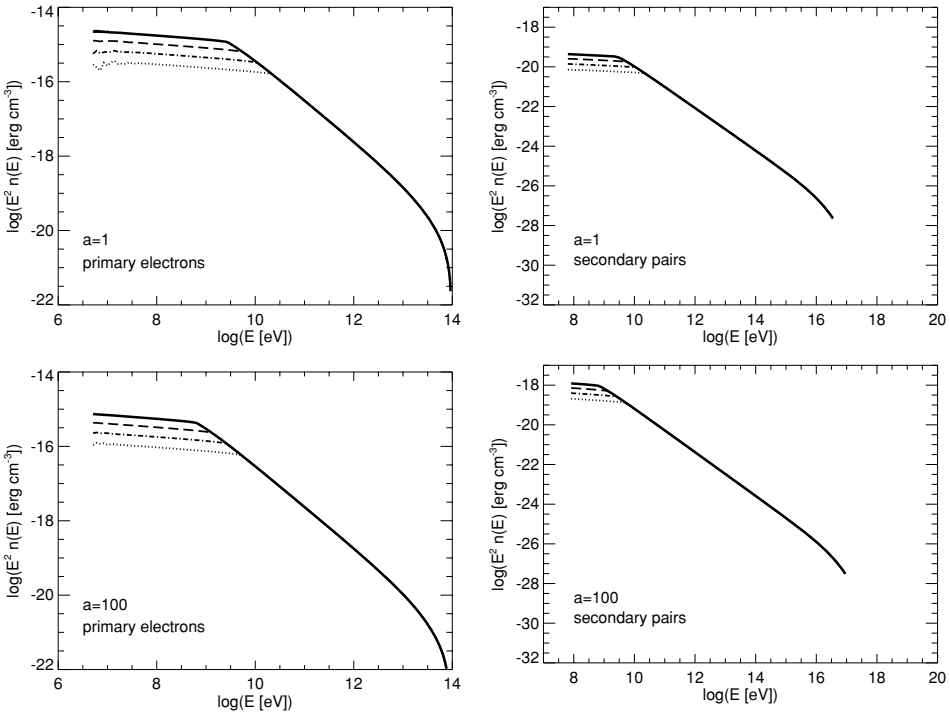

Figure 2. Spectral energy distributions of primary electrons and secondary pairs for $a = 1$ (upper panels) and $a = 100$ (lower panels). Distributions for different particle injection time-scales ($\tau_{\rm shock}$) are shown in each panel. Different curves correspond to the following values of $\tau_{\rm shock}$: 0.125 Gyr (dotted line), 0.25 Gyr (dot–dashed line), 0.5 Gyr (dashed line) and 1 Gyr (solid line). The steady regime is reached for ages $\sim \tau^{\rm relic}_{\rm shock}$.

($\tau_{pp} \sim 10^3$ Gyr). Consequently, the energy distribution in the context of our scenario keeps the same spectral shape as that of the injected one. Since $\tau_{\rm esc}$ is of the order of $\tau^{\rm relic}_{\rm shock}$, we can consider that the energy distribution of protons also reaches the steady regime at $\tau^{\rm relic}_{\rm shock}$.

All these calculations give us the steady energy distribution of the different population of relativistic particles, i.e. primary electrons, secondary pairs and protons, that have become part of the relics. Electrons are responsible for the radio emission of the cluster A3376 observed in its giant ring-like radio structures. As we have shown, this emission has been used to estimate the magnetic field strength in the acceleration region, and the normalization and maximum energies involved in the power laws that represent the particle energy distributions. In the following section, we estimate the contribution of both relativistic leptons and protons to the high-energy emission of the cluster, evaluating the detectability of A3376 in the MeV–TeV electromagnetic range.

4 PRODUCTION OF GAMMA-RAYS AND LOWER ENERGY RADIATION

Using the steady distributions of particles estimated in the previous section, we calculate the SEDs for the three different combinations of proton and lepton relativistic energy densities (i.e. cases $a = 0$, 1, 100). We take into account the most relevant non-thermal radiative processes according to the conditions of the ambient medium in the cluster A3376.

4.1 Leptonic emission

The differential emissivities $q_\gamma(E_\gamma)$ produced by leptons for synchrotron radiation, IC scattering and relativistic Bremsstrahlung are calculated using the standard formulae given by Blumenthal & Gould (1970) and Pacholczyk (1970). The luminosity produced in the relics is given by the equation

$$E_\gamma L_{E_\gamma} = E_\gamma^2\, q_\gamma(E_\gamma)\, V_{\rm relic}, \tag{13}$$

where E_γ is the photon energy and $v_{\rm relic}$ is the volume of the emitting region. For the latter, we adopt a value of $\sim$0.09 Mpc^3, as we have mentioned in Section 2. In the cases where a population of accelerated protons is assumed to be present ($a = 1$, 100), we estimate the contribution of secondary pairs to the SEDs for completitude.

Results of the luminosity produced in the case where only primary electrons are accelerated, characterized by $a = 0$, are shown in Fig. 3. We can see that IC interactions are the dominant process, with a luminosity $L_{\rm IC} \sim 9.1 \times 10^{41}$ erg s^{-1}, at energies $E_\gamma \gtrsim 0.1$ MeV and with a cut-off at $\sim$10 TeV. The luminosity produced by relativistic Bremsstrahlung is negligible, in agreement with results shown in Fig. 1.

4.2 Hadronic emission

Proton–proton interactions produce gamma-ray emission through π^0-decay. The corresponding differential gamma-ray emissivity is calculated as

$$q_\gamma(E_\gamma) = 2\int_{E_\pi^{\rm min}(E_\gamma)}^{\infty} \frac{q_{\pi^0}(E_\pi)}{\sqrt{E_\pi^2 - m_\pi^2 c^4}}\, {\rm d}E_\pi, \tag{14}$$

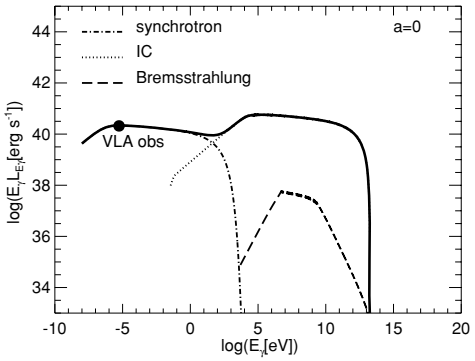

Figure 3. SED for a pure leptonic case ($a = 0$), represented by a solid line. The contribution of different radiative processes is shown: synchrotron radiation (dot–dashed line), IC scattering (dotted line) and relativistic Bremsstrahlung (dashed line). The VLA observation at 1.4 GHz is also included.

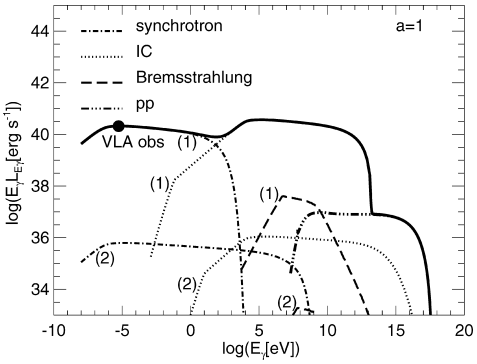

Figure 4. SED for a mixed primary population of relativistic electrons and protons characterized by $a = 1$, represented by a solid line. The contribution of different radiation processes is identified as in Fig. 3. The contribution from secondary pairs is also included.

where $E_\pi^{\rm min}(E_\gamma) = E_\gamma + m_\pi^2 c^4/4E_\gamma$. Applying the δ-functional approximation for the differential cross-section[1] (Aharonian & Atoyan 2000), the pion emissivity becomes

$$q_{\pi^0}(E_\pi) = \frac{4\pi}{\kappa}\, n_{\rm H}\, J_{\rm p}\left(m_{\rm p}c^2 + \frac{E_\pi}{\kappa}\right)\sigma_{pp}\left(m_{\rm p}c^2 + \frac{E_\pi}{\kappa}\right) \tag{15}$$

for proton energies greater than the energy threshold $E_{\rm th} = 1.22$ GeV and lower than 100 GeV. Here, κ is the mean fraction of the kinetic energy $E_{\rm kin} = E_{\rm p} - m_{\rm p}c^2$ of the proton transferred to a secondary meson per collision. For a broad energy region (GeV to TeV) we have that $\kappa \sim 0.17$. The proton flux is given by $J_{\rm p}(E_{\rm p}) = (4\pi/c)\, n(E_{\rm p})$. The total cross-section of the inelastic *pp* collisions is given by equation (9). For $E_{\rm p} > 100$ GeV, the equations given by Kelner et al. (2006) are used. The specific luminosity is estimated in the same way as for electrons (equation 13).

The results of our calculations for the case $a = 1$ are shown in Fig. 4. Just as the case characterized by $a = 0$, the SED is dominated by the IC interactions, with a luminosity $L_{\rm IC} \sim 7.4 \times 10^{41}$ erg s^{-1}. The emission at energies higher than $\sim$1 GeV is produced by neutral

[1] This approximation considers only the most energetic neutral pion that is produced in the *pp* reaction aside of a *fireball* composed by a certain number of less energetic π-mesons of each flavour. See a discussion in Pfrommer & Enßlin (2004).

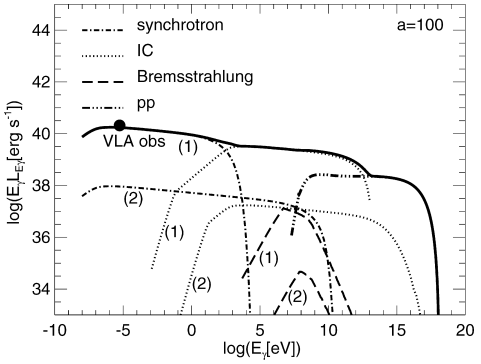

Figure 5. Idem as Fig 4, but for a case dominated by relativistic protons ($a = 100$).

pion decay, reaching a luminosity $L_{pp} \sim 1.6 \times 10^{38}$ erg s^{-1} with a cut-off at $E_\gamma \sim 10^{17}$ eV. However, its contribution to the SED becomes evident at energies $\gtrsim$10 TeV.

In the case corresponding to $a = 100$, the relativistic energy density of protons is higher than that of the primary electrons. However, the proton dominance does not imply necessarily a significant increase in photon production from *pp*-interactions because of the low density of thermal protons at the location of radio relics. Hence, the power produced by π^0-decay does not dominate the SEDs, as can be seen in Fig. 5. The luminosity L_{pp} is of the order of $\sim$4.2 $\times$ 10^{39} erg s^{-1}, being slightly larger than the one corresponding to the case with $a = 1$. In contrast to the cases with $a = 0$ and 1, the IC emission is lower than the synchrotron one, with luminosities $L_{\rm IC}$ $\sim 7.1 \times 10^{40}$ and $L_{\rm synch} \sim 3.8 \times 10^{41}$ erg s^{-1}, respectively. The fact that radiation produced by IC scattering is reduced for the case $a =$ 100 might be explained as a consequence of equipartition between the magnetic field and the particle energy density. As can be seen in Table 1, the magnetic field becomes larger as the value of a increases. This will reduce the amount of electron energy released via IC scattering with respect to that released via synchrotron. In addition, the available electron energy is also reduced to explain the radio fluxes due to the larger magnetic field. All this makes the IC luminosity smaller. Concerning the emission produced by secondary pairs, we find that their contributions to the SEDs by different radiation processes are larger than that for the case $a = 1$, but are still irrelevant. This is consistent with the low efficiency of *pp*-interactions taking place in the outskirts of the cluster.

4.3 Gamma-ray emission

The SED shown in Figs 3 to 5 is built considering the contribution of different non-thermal radiative processes in a wide range of energies, from radio to gamma-rays. In this work, we are particularly interested in the detectability of the cluster A3376 at gamma-ray energies. We find that the main processes contributing to the emission at these high energies are IC scattering and π^0-decay, being the luminosity of the latter considerably smaller even for the case where a large energy density of protons is considered. The HESS array could detect the estimated emission from A3376 in exposure times between 1 d to 1 month, for different values of a. On the other hand, more than 1 yr is necessary to detect with GLAST the non-thermal gamma-ray emission estimated for the cluster studied in this work. However, small changes in the assumptions of our model can yield higher fluxes that would result in a considerably reduction of the exposure time for detection. For instance, if subpartition between magnetic and relativistic particle energy densities is considered instead of equipartition, there would be an increase in the IC emission. Thus, if the IC luminosity of A3376 is $L_{\rm IC} \sim 10^{42}$ erg s^{-1} at energies above 100 MeV it would be detected by GLAST in less than 1 yr (i.e. within the initial all-sky survey). Finally, photons produced by *pp*-interactions could might be by the future Cherenkov telescope HESS II on short time-scales.

5 SUMMARY AND PROSPECTS

We have presented a model for the emission produced by the nearby cluster A3376 in a wide range of energies, from radio to gamma-rays, considering the contribution of different non-thermal radiative processes. This cluster presents strong evidence of merger activity, characterized by large-scale ring-shaped synchrotron radio structures, which are identified with radio relics (Bagchi et al. 2006). These kind of radio structures detected in several clusters of galaxies suggests a rich content of accelerated particles in the ICM, with energies as high as $\sim 10^{14}$ and $\sim 10^{18}$ eV for electrons and protons, respectively. Taking into account that radio relics are tracers of merger shocks, we assume that a diffusive shock acceleration mechanism acting at the wave shocks gives place to such a population of relativistic particles. These particles are subsequently cooled by different leptonic and hadronic radiative processes.

We have considered syncrotron radiation, IC scattering and relativistic Bremsstrahlung that affect relativistic primary electrons. Relativistic protons are involved in *pp*-interactions with the thermal protons of the ICM. This process gives raise to a population of secondary pairs, $e^{\pm}$, that are cooled by the same processes that affect the population of primary electrons. The parameters involved in these non-thermal processes, such as the magnetic field and normalization of the energy distribution of accelerated particles, have been estimated from the constraints established by the observed radio power in the relics and the assumption of equipartition. X-ray observations allow us to extract information about the volume of these acceleration sources. On the other hand, results from a simulated cluster have provided the typical gas density of the relics and the velocity of this shock.

We find that particle energy distributions reach a stationary regime by the lifetime of the relics ($\sim$1 Gyr). The steady energy distribution of particles is computed and the SEDs of the radiation produced at the relic position derived. In our calculations, we have adopted different ratios ($a = 0$, 1, 100) for the relativistic proton/electron energy densities. At larger energies, gamma-ray emission is mainly produced by π^0-decay but with a considerably smaller luminosity, even for the case where a large energy density of protons is considered ($L_{pp} \sim 4 \times 10^{39}$ erg s^{-1}). This is consistent with the fact that no cluster has been yet observed at these high energies.

The proximity of the cluster studied in this paper and its high content of relativistic particles in the radio relics make A3376 an interesting potential target for the investigation of gamma-ray emission in this type of objects. This source might be detected at gamma-rays by GLAST satellite and by HESS array with a reasonable exposure time. In addition, future Cherenkov telescopes in the southern hemisphere, like HESS II, could easily detect the high-energy emission from A3376.

ACKNOWLEDGMENTS

We are grateful to an anonymous referee for insightful remarks. We thank Valentí Bosch-Ramon for helpful discussion and comments

about this work. Marcus Brüeggen is acknowledged for useful remarks. ATA and GER are supported by CONICET (PIP 5375) and the Argentine agency ANPCyT through Grant PICT 03-13291 BID 1728/OC-AC. SAC is supported by CONICET (PIP 5000/2005) and the Argentine agency ANPCyT through Grant PICT 26049 BID 1728/OC-AC.

REFERENCES

Aharonian F. A., Atoyan A. M., 2000, A&A, 362, 937
Atoyan A. M., Völk H. J., 2000, ApJ, 535, 45
Bagchi J., Durret F., Neto G. B. L., Paul S., 2006, Sci, 314, 791
Balestra I., Tozzi P., Ettori S., Rosati P., Borgani S., Mainieri V., Norman C., Viola M., 2007, A&A, 462, 429
Berezinsky V. S., Grigorieva S. I., 1988, A&A, 199, 1
Berrington R. C., Dermer C. D., 2003, ApJ, 594, 709
Blasi P., 2003, in Bowyer S., Hwang C.-Y., eds, ASP Conf. Ser. Vol. 301, Gamma Rays from Clusters of Galaxies. Astron. Soc. Pac., San Francisco, p. 203
Blumenthal G. R., Gould R. J., 1970, Rev. Mod. Phys., 42, 237
Bowyer S., Korpela E. J., Lampton M., Jones T. W., 2004, ApJ, 605, 168
Churazov E., Forman W., Jones C., Böhringer H., 2000, A&A, 356, 788
Dolag K., Vazza F., Brunetti G., Tormen G., 2005, MNRAS, 354, 753
Domainko W., Benbow W., Hinton J. A., Martineau-Huynh O., de Naurois M., Nedbal D., Pedaletti G., Rowell G., 2007, for the HESS Collaboration, 30th International Cosmic Ray Conference. Merida, Mexico, preprint (astro-ph/0708.1384v1)
Drury L. O., 1983, Rep. Prog. Phys., 46, 973
Enßlin T. A., Biermann P. L., 1998, A&A, 330, 90
Enßlin T. A., Gopal-Krishna, 2001, A&A, 366, 26
Enßlin T. A., Biermann P. L., Klein U., Kohle S., 1998, A&A, 332, 395
Fegan S. J. et al., 2005, ApJ, 624, 638
Feretti L., Givannini G., 1996, in Ekers R., Fanti C., Padrielli Ĺ., eds, Proc. IAU Symp. 175, Extragalactic Radio Sources. Kluwer Academic Publisher, Dordrecht, p. 333
Feretti L., Giovannini G., 2008, in Plionis M., Lopez-Cruz O., Hughes D., eds, Panchromatic View of Clusters of Galaxies and the Large-Scale Structure. Lecture Notes Physics 740. Springer, Dordrecht, p. 143
Feretti L., Böhringer H., Giovannini G., Neumann D., 1997, A&A, 317, 432
Feretti L., Fusco-Femiano R., Giovannini G., Govoni F., 2001, A&A, 373, 106
Feretti L., Burigana C., Enßlin T. A., 2004, New Astron. Rev., 48, 1137
Fusco-Femiano R., dal Fiume D., Feretti L., Giovannini G., Grandi P., Matt G., Molendi S., Santangelo A., 1999, ApJ, 513, L21
Fusco-Femiano R., Orlandini M., Brunetti G., Feretti L., Giovannini G., Grandi P., Setti G., 2004, ApJ, 602, L73
Gabici S., Blasi P., 2003, ApJ, 583, 695
Ginzburg V. L., Syrovatskii S. I., 1964, The Origin of Cosmic Rays. Pergamon Press, New York
Giovanninii G., Ferreti L., 2004, J. Korean Astron. Soc., 37, 323
Giovannini G., Feretti L., Stanghellini C., 1991, A&A, 252, 528
Girardi M., Giuricin G., Mardirossian F., Mezzetti M., Boschin W., 1998, ApJ, 505, 74
Govoni F., Feretti L., 2004, Int. J. Mod. Phys. D, 13, 1549
Govoni F. F. L., Giovannini G., Böhringer H., Reiprich T. H., Murgia M., 2001, A&A, 376, 803
Hoeft M., Brüeggen M., Yepes G., 2004, MNRAS, 347, 389
Jaffe W. J., 1977, ApJ, 212, 1
Khangulyan D., Hnatic S., Aharonian F., Bogovalov S., 2007, MNRAS, 380, 312
Kelner S. R., Aharonian F. A., 2008, Phys. Rev. D, in press (arXiv:0803.0688v1)
Kelner S. R., Aharonian F. A., Vugayov V. V., 2006, Phys. Rev. D, 74, 034018
Keshet U., Waxman E., Loeb A., Springel V., Hernquist L., 2003, ApJ, 585, 128
Lieu R., Mittaz J. P. D., Bowyer S., Lockman F., Hwang C.-Y., Schmitt J. H. M. M., 1996, ApJ, 458, L5
Lieu R., Axford W. I., Bonamente M., 1999, ApJ, 510, L25
Mannheim K., Schlickeiser R., 1994, A&A, 286, 983
Mittaz J. P. D., Lieu R., Lockman F. J., 1998, ApJ, 498, L17
Pacholczyk A. G., 1970, Radio Astrophysics. Freeman, San Francisco
Perkins J. S. et al., 2006, ApJ, 644, 148
Petrosian V., 2001, ApJ, 557, 560
Pfrommer C., Enßlin T. A., 2004, A&A, 413, 17
Pfrommer C., Springel V., Enßlin T. A., Jubelgas M., 2006, MNRAS, 367, 113
Pfrommer C., Enßlin T. A., Springel V., Jubelgas M., Dolag K., 2007, MNRAS, 378, 385
Pfrommer C., Enßlin T. A., Springel V., 2008, MNRAS, 385, 1211
Reimer O., Pohl M., Sreekumar P., Mattox J. R., 2003, ApJ, 588, 155
Röttgering H. J. A., Snellen I., Miley G., de Jong J. P., Hanisch R. J., Perley R., 1994, ApJ, 436, 654
Röttgering H. J. A., Wieringa M. H., Hunstead R. W., Ekers R. D., 1997, MNRAS, 290, 577
Völk H. J., Aharonian F. A., Breitschwerdt D., 1996, Space Sci. Rev., 75, 279

This paper has been typeset from a TEX/LATEX file prepared by the author.